Electro paramagnetic resonance and optical spectra of Ti^{3+}-doped $YAlO_3$

1992 J. Phys.: Condens. Matter 4 7285

(http://iopscience.iop.org/0953-8984/4/35/011)

J. Phys.: Condens. Matter 4 (1992) 7285–7294. Printed in the UK

Electron paramagnetic resonance and optical spectra of Ti^{3+}-doped $YAlO_3$

M Yamaga†, T Yosida‡, B Henderson§, K P O'Donnell§ and M Date||

† Department of Physics, Faculty of General Education, Gifu University, Gifu 501-11, Japan

‡ Low Temperature Centre, Osaka University, Toyonaka 560, Japan

§ Department of Physics and Applied Physics, University of Strathclyde, Glasgow G4 0NG, UK

|| Department of Physics, Faculty of Science, Osaka University, Toyonaka 560, Japan

Received 23 April 1992

Abstract. The electron paramagnetic resonance (EPR), optical absorption and luminescence spectra of Ti^{3+} ions in $YAlO_3$ have been measured at low temperatures. The optical absorption spectrum is composed of two broad bands with peak wavelengths of 434 and 492 nm, the energy separation of which is due to splitting of the excited ^2E state. The broad-band luminescence with a peak at a wavelength of 605 nm at low temperatures is accompanied by a single sharp zero-phonon line at 540 nm. The absorption and luminescence spectra are strongly polarized. The spin-Hamiltonian parameters of Ti^{3+} ions substituting for Al^{3+} ions in sites with orthorhombic symmetry were determined from the orientation dependence of the EPR spectra to be $g_x = 1.795(5)$, $g_y = 1.850(5)$ and $g_z = 1.950(5)$. The experimental g-tensor is compared with that calculated in terms of the mixing of the higher components of the $^2T_2$ ground states and the ^2E excited states into the lowest $^2T_2$ ground state by spin–orbit interaction, the energies of these levels having been estimated from the broad-band absorption spectrum and the zero-phonon lines of the emission spectrum.

1. Introduction

Yttrium aluminium perovskite (YAP) $YAlO_3$ is a host crystal which supports laser action when containing rare-earth ions (Nd^{3+}, Tm^{3+} or Er^{3+}) [1]. The transition-metal ion Cr^{3+} in YAP is used to sensitize Nd^{3+} luminescence via energy transfer from Cr^{3+} ions excited in the broad-band absorption to Nd^{3+} ions. The pumping efficiency for the Nd^{3+} laser action of Cr^{3+}-codoped Nd^{3+}:YAP is higher than that for Nd^{3+}:YAP [2]. The luminescence from Cr^{3+} ions in YAP, observed at room temperature, consists of the sharp R lines and their phonon sidebands [3]. The Cr^{3+}:YAP laser operates on the sharp R lines as do the Cr^{3+}:Al_2O_3 and Cr^{3+}:$Y_3Al_5O_{12}$ (YAG) lasers. Recently, Ti^{3+}-doped YAP [4–6] has attracted considerable interest in view of its potential as a solid state laser material operating at shorter wavelengths than Ti^{3+}:Al_2O_3 (sapphire) does. Laser operation has not been successful because of the excited-state absorption involving higher energy levels than those of the ^2E excited states [5, 6].

The optical absorption and luminescence from the laser-active ions such as Nd^{3+}, Cr^{3+} and Ti^{3+} depend strongly on the structure of the host crystals. The crystal structure of YAP has a distorted orthorhombic symmetry [7, 8]. In consequence,

0953-8984/92/357285+10$04.50

optical transitions between the excited and ground states have an electric dipole nature and both the absorption and the luminescence spectra are strongly polarized. For example, the 1.08 μm emission line in Nd^{3+}:YAP is polarized parallel to the *c* axis, whereas the 1.065 μm line is polarized parallel to the *b* axis [9]. The anisotropies of the optical absorption spectra of Cr^{3+}:YAP [10] and of the emission spectra of Ti^{3+}:YAP [11, 12] have been reported. This paper discusses the anisotropy of the YAP crystal determined using electron paramagnetic resonance (EPR) and the polarization of the optical absorption spectra of the paramagnetic ion Ti^{3+}. The **g**-tensor and optical polarization measured are strongly related to the crystal structure.

2. Crystal structure of $YAlO_3$

YAP has a slightly distorted perovskite structure, the crystals belonging to the space group D_{2h}^{16} ($Pbnm$). X-ray diffraction measurements have been reported by Geller and Wood [7]. Subsequently, the crystallographic parameters were refined by Diehl and Brandt [8]. The projection of two unit cells along the *c* axis is shown in figure 1. The distances between the central Al ion and the three oxygen ions (I), (II) and (III) in figure 1 were determined from x-ray measurement to be 1.911 Å, 1.921 Å and 1.901 Å, respectively. The octahedron compressed along the Al^{3+}–O(III) direction has pseudo-tetragonal symmetry. In Ti^{3+}:YAP the Al^{3+} ions at the centre of an octahedral arrangement of oxygen ligands may be replaced by Ti^{3+} ions. In consequence, there are four crystallographically inequivalent Ti^{3+} sites, as shown in figure 1.

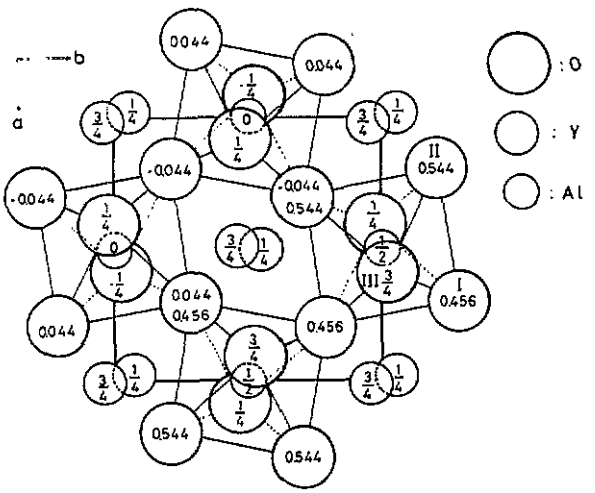

Figure 1. Orthogonal projection of two unit cells of YAP onto the (001) plane.

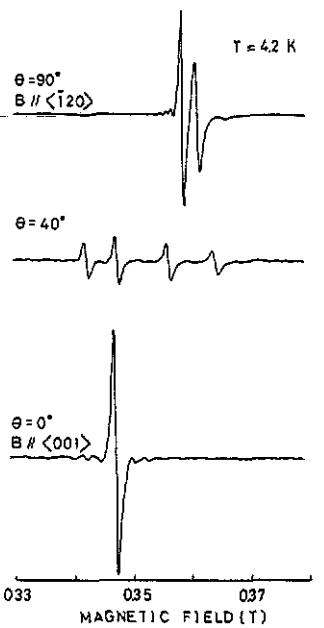

Figure 2. EPR spectra of Ti^{3+}:YAP with magnetic fields applied parallel to the [001] and [$\bar{1}$20] directions and at 40° from [001] to [$\bar{1}$20].

3. Experimental procedure and results

Ti^{3+}-doped single crystals were grown by the Czochralski technique. Samples with approximate dimensions 1 mm × 2 mm × 5 mm were cut from the single crystal, the cut faces being normal to the [210], [$\bar{1}$20] and [001] (*c*-axis) direction of the crystal. The EPR measurements were made at temperatures in the range 4.2–77 K using a Varian X-band EPR spectrometer employing 270 Hz field modulation. The polarizations of the optical absorption spectra of the Ti^{3+} ions were measured at room temperature by inserting a linear polarizer in an optical spectrometer at the Centre of Instrumentation, Gifu University. The luminescence emitted in a direction perpendicular to the excitation direction was detected through a 1 m grating monochromator using a GaAs phototube and a current amplifier. The sample temperature was controlled in the range 10–300 K using a cryorefrigerator.

3.1. EPR measurements

The EPR transitions of Ti^{3+} in YAP are relatively easily saturated at the cryogenic temperature (about 4.2 K), even at low microwave power levels. Figure 2 shows the EPR spectra measured at a microwave power of 0.01 mW and a microwave frequency of 9.302 GHz. In these measurements the magnetic field was applied parallel to the [001] and [$\bar{1}$20] directions and at 40° from the [001] towards the [$\bar{1}$20] direction. The EPR spectrum at $\boldsymbol{B}\|[001]$ is revealed as a single resonance line with several weak satellite lines, associated with hyperfine structure due to the nuclear spin of isotopes ^{47}Ti ($I = \frac{5}{2}$) and ^{49}Ti ($I = \frac{7}{2}$) with natural abundances of 7.3% and 5.5%, respectively. Figure 3 shows the angular dependence of the EPR spectra as the magnetic field is rotated in the (001) and (210) planes. The open circles in figure 3 represent the field positions of the resonance lines. The EPR spectra at some magnetic field directions consist of four resonance lines. The four lines converge to a single line when the applied magnetic field is parallel to the [100], [010] and [001] directions, i.e. the *a*, *b* and *c* axes (see figure 1). These results indicate that the EPR signals are due to four inequivalent sites which become equivalent when the magnetic field is parallel to the *a*, *b* and *c* axes.

The angular dependences of the EPR spectra are fitted by the spin Hamiltonian

$$H = g_x \mu_B S_x B_x + g_y \mu_B S_y B_y + g_z \mu_B S_z B_z \tag{1}$$

where $S = \frac{1}{2}$, and μ_B is the Bohr magneton [13–15]. The principle axes x, y and z of the **g**-tensor and the polar angles (θ_x, ϕ_x) for the x axis and (θ_z, ϕ_z) for the z axis are defined with respect to the (a, b, c) co-ordinate system in figure 4. The full curves in figure 3, calculated using equation (1) with the spin-Hamiltonian parameters and the polar angles of the principal axes listed in table 1, fit the angular variations in the EPR signals.

Figure 5(*a*) shows the temperature dependence of the EPR spectra for $\boldsymbol{B}\|[210]$. The peak-to-peak intensities of the signals decrease rapidly with increasing temperature and are not detected above 70 K as a consequence of line broadening. The linewidth is associated with spin–lattice relaxation [13–15]. We assume that, as temperature increases, only the linewidth of the EPR line broadens, the microwave absorption power integrated over the field remaining constant, and that a microwave absorption lineshape as a function of magnetic field is given by the first derivative of a Lorentzian. Then, the linewidth is inversely proportional to the square root of the

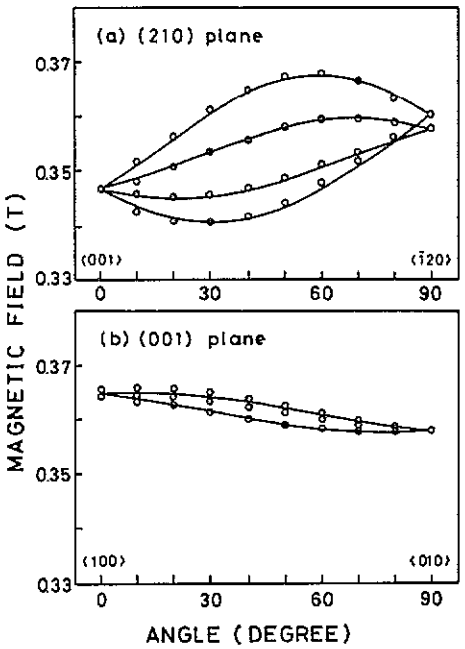

Figure 3. Angular dependence of the EPR spectra of Ti^{3+}:YAP at 4.2 K with the magnetic field in (*a*) the (210) plane and (*b*) the (001) plane: ——, calculated using equation (1) and the spin-Hamiltonian parameters in table 1.

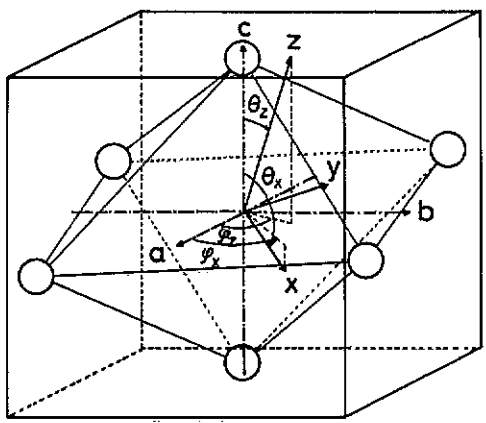

Figure 4. Principal axes x, y, z, and their polar angles of one of four Ti^{3+} octahedra with respect to the a, b, c coordinate system.

Table 1. Spin-Hamiltonian parameters and polar angles of the principal axis directions of Ti^{3+} ions in YAP.

Crystal	g_x	g_y	g_z	θ_x (deg)	ϕ_x (deg)	θ_z (deg)	ϕ_z (deg)
Ti^{3+}:YAP	1.795(5)	1.850(5)	1.950(5)	117(2)	31(2)	30(2)	60(2)

peak-to-peak intensity of the first-derivative curve. Figure 5(*b*) shows the linewidth $\Gamma(T)$, normalized by $\Gamma(11)$, as a function of the temperature T. The linewidth increases abruptly above $T = 40$ K.

3.2. Optical measurements

Figure 6 shows the polarized absorption spectra of Ti^{3+}:YAP measured at room temperature. Each absorption spectrum consists of two broad bands associated with the splitting of ^2E excited states by an orthorhombic distortion [16]. The peak wavelengths of the two bands are at 434 nm (denoted by A) and at 492 nm (denoted by B); the peaks are strongly polarized along the [010] direction (*b* axis). Figure 7 shows the variation in the absorption coefficients at orientations in the (001) and (010) planes at the peak wavelengths of the two bands, after subtraction of the background signal. Band B is nearly isotropic, whereas the intensity of band A for $E\|[010]$ (*b* axis) is approximately twice that for $E\|[001]$ (*c* axis).

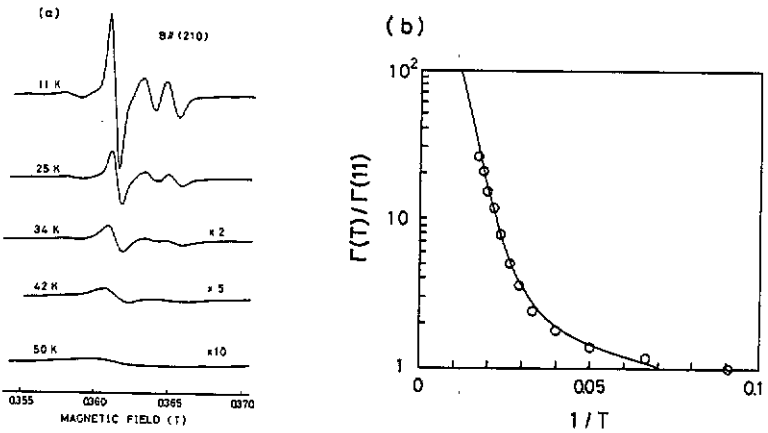

Figure 5. (*a*) Temperature dependence of the EPR spectra of Ti^{3+}:YAP at $B\|[210]$: ——, calculated using equation (7) and the parameters $a' = 0.072$, $c' = 1700$ and $\delta_1 = 170\ cm^{-1}$. (*b*) Temperature dependence of the linewidth $\Gamma(T)$ of the EPR spectra normalized by $\Gamma(11)$.

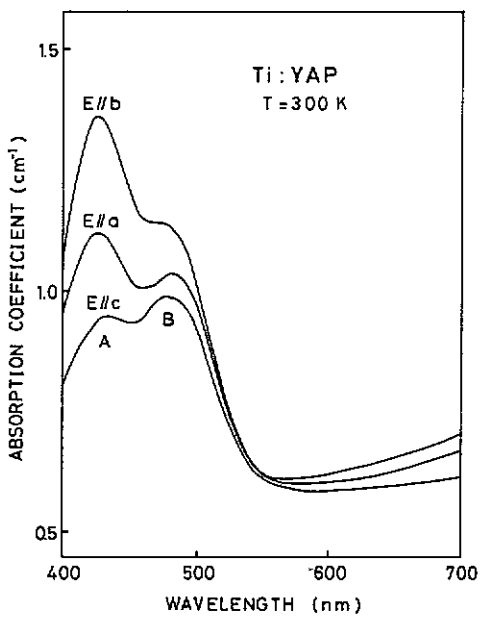

Figure 6. Polarization of absorption spectra of Ti^{3+}:YAP observed at room temperature.

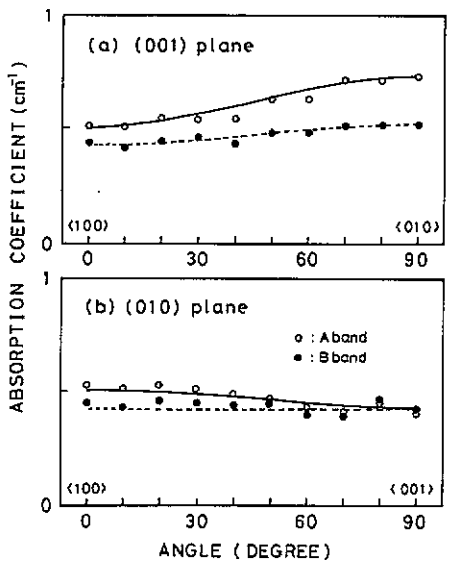

Figure 7. Angular variation in absorption coefficients at the peak wavelengths 434 nm (band A) and 492 nm (band B), being polarized (*a*) in the (001) and (*b*) in the (010) planes observed for Ti^{3+}:YAP at room temperature: ——, calculated using equation (2) for the broad band A; – – –, calculated using equation (2) for the broad band B.

The orientation dependence of the polarization can be calculated in terms of electric dipole moment operators er between the ground and excited states [11], using the principal axes x, y and z of the Ti^{3+} complex determined from the EPR

measurements. The x, y and z components of the transition probability due to the ex, ey and ez electric dipole moment operators are defined as A_x, A_y and A_z, respectively, for absorption. The broad-band absorption polarized along one crystal direction, including the contribution from four crystallographically inequivalent Ti^{3+} sites in figure 1, is given by

$$P = \sum_{k=1}^{4} A_x \cos^2 \theta_{kx} + A_y \cos^2 \theta_{ky} + A_z \cos^2 \theta_{kz} \tag{2}$$

where θ_{kx}, θ_{ky} and θ_{kz} are the angles between the E-vector direction of absorption light and the principal axes x, y and z of the kth Ti^{3+} site respectively. The full and broken curves in figure 7 are calculated using equation (2) and the parameters $A_x : A_y : A_z = 0.3 : 1 : 0.45$ and $A_x : A_y : A_z = 0.55 : 1 : 0.75$ for the two broad bands A and B, respectively. The A_y-components are dominant for both band A and band B.

Figure 8 shows the luminescence spectrum from Ti^{3+} in YAP observed at 10 K. The inset in figure 8 shows the zero-phonon emission line at 540 nm and the associated one-phonon sidebands. The luminescence spectrum is polarized along the [110] direction [12].

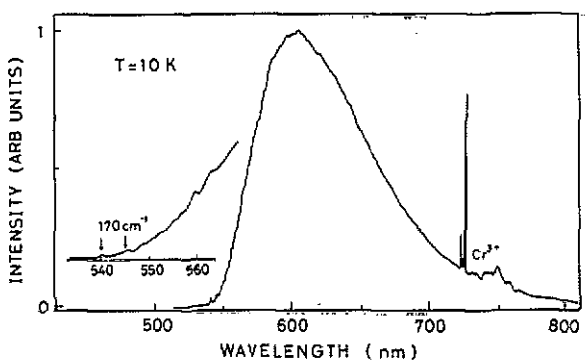

Figure 8. Luminescence spectrum of Ti^{3+}:YAP observed at 10 K. The inset shows a zero-phonon emission line and the phonon sidebands. The luminescence at the long-wavelength tail of the Ti^{3+} broad-band emission is due to the accidental doping with Cr^{3+} ions.

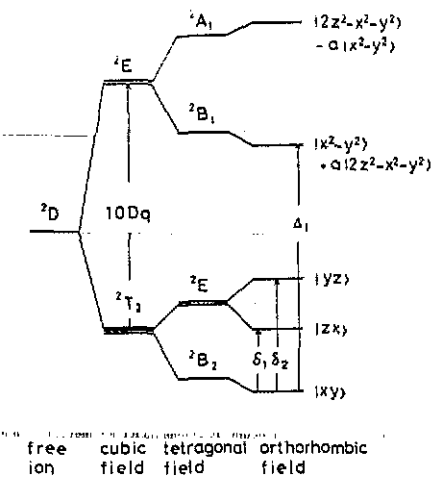

Figure 9. Energy diagram of Ti^{3+} in cubic, tetragonal and orthorhombic symmetries.

4. Discussion

Ti^{3+} has the electron configuration $3d^1$ [17]. Figure 9 shows the energy-level scheme of octahedrally coordinated Ti^{3+} ions in the presence of cubic, tetragonal or orthorhombic crystal-field distortions. The ^2D state of $3d^1$ ions in an octahedral field

splits into the $^2T_2$ ground state and the ^2E excited state with energy separation $10Dq$. In tetragonal symmetry, the $^2T_2$ ground state is further split into the $^2B_2$ ($|xy\rangle$) and ^2E ($|yz\rangle, |zx\rangle$) states. Which of the orbital doublet (^2E) or the singlet ($^2B_2$) is the lower is determined by whether the octahedron is elongated or compressed, respectively, along the z axis. The ^2E excited state is split further into A_1 ($|2z^2 - x^2 - y^2\rangle$) and B_1 ($|x^2 - y^2\rangle$) states by tetragonal distortion. If the complex of the Ti^{3+} ion is compressed, the B_1 state is lower in energy. The $^2T_2$ state in orthorhombic symmetry splits into three non-degenerate orbital states. The lowest excited state in orthorhombic symmetry is represented by a linear combination of the A_1 and B_1 states. The mixing coefficients are determined by the strength of the crystal field perpendicular to the dominant tetragonal field.

The structures of zero-phonon emission lines and the absorption spectra reflect the energy levels of the $^2T_2$ ground states and the ^2E excited states of Ti^{3+}:YAP in an orthorhombic crystal field, respectively. The single zero-phonon emission line from Ti^{3+}:YAP was observed at 540 nm as shown in figure 8. This feature is different from that in Ti^{3+}:Al_2O_3, where two zero-phonon emission lines are observed because of the splitting of the fourfold-degenerate ^2E lowest ground state in the trigonal crystal field by a spin–orbit interaction [12, 18]. These results indicate that the lowest ground state in Ti^{3+}:YAP is a Kramers doublet. However, which of the $|xy\rangle$, $|yz\rangle$ or $|zx\rangle$ orbital states is the lowest component of the $^2T_2$ ground state cannot be determined from the zero-phonon line. It may, however, be deduced from the **g**-tensor of Ti^{3+}. The energy separation of the two absorption bands can be used to estimate the splitting of the ^2E excited state but do not determine the mixed wavefunctions of the excited states in orthorhombic symmetry.

The Ti^{3+} octahedron in YAP is nearly tetragonal. Yamaga *et al* [11] have calculated the transition probabilities induced by odd-parity distortion, T_{1u}, between the ground and excited states of Ti^{3+} in axial symmetry (tetragonal and trigonal). We apply that theory to the polarization of the absorption spectra of Ti^{3+} in YAP. First, we describe briefly the results of their calculations. Electric dipole transitions between the $|xy\rangle$ ground state and the $|x^2 - y^2\rangle$, $|2z^2 - x^2 - y^2\rangle$ excited states in sites with tetragonal symmetry are not induced by the z component of T_{1u} odd-parity distortion. However, the x and y components of this distortion do induce y- and x-polarized electric dipole transitions, respectively. The probability of transition between $|xy\rangle$ and $|x^2 - y^2\rangle$ orbitals is three times that between $|xy\rangle$ and $|2z^2 - x^2 - y^2\rangle$. The ez electric dipole transitions induced by the x and y components of T_{1u} occur between the $|yz\rangle$, $|zx\rangle$ ground states and the $|x^2-y^2\rangle$, $|2z^2-x^2-y^2\rangle$ excited states. The x, y and z components of the transition probabilities for the two absorption bands A and B, being proportional to absorption coefficients, were experimentally determined to be $A_x : A_y : A_z = 0.3 : 1 : 0.45$ and $A_x : A_y : A_z = 0.55 : 1 : 0.75$, respectively. Comparing the experimental results for both band A and band B shows that A_y is dominant and A_z is greater than zero. As the theory indicates that the (x, y) and z components of the polarization are associated with the transitions from the $|xy\rangle$ and ($|yz\rangle$, $|zx\rangle$) ground states, respectively, the lowest ground state may be $|xy\rangle$ with small admixtures of the $|yz\rangle$ and $|zx\rangle$ states. However, the small difference between the experiment and the calculated polarization for tetragonal symmetry may be due to orthorhombic symmetry which mixes the wavefunctions between the three orbital states of the ground states and between the two orbital states of the excited states, resulting in the complex polarization.

The g-factors for the pure $|xy\rangle$ ground state of Ti^{3+} in orthorhombic symmetry

[15, 19, 20] are calculated in terms of the spin–orbit perturbation with the assumption that the lowest excited state of ^{2}E in figure 9 is pure $|x^2 - y^2\rangle$ and given by

$$g_x = 2 - 2\lambda/\delta_1 + \lambda^2/2\delta_1^2 - \lambda^2/2\delta_2^2 + 2\lambda^2/\delta_2\Delta_1 - 2\lambda^2/\Delta_1^2 \quad (3)$$

$$g_y = 2 - 2\lambda/\delta_2 - \lambda^2/2\delta_1^2 + \lambda^2/2\delta_2^2 + 2\lambda^2/\delta_1\Delta_1 - 2\lambda^2/\Delta_1^2 \quad (4)$$

$$g_z = 2 - 8\lambda/\Delta_1 - \tfrac{1}{2}(\lambda/\delta_1 + \lambda/\delta_2)^2 + 2\lambda^2/\Delta_1^2 \quad (5)$$

where $\lambda(= k\zeta)$ is an effective spin–orbit parameter, k is the orbital reduction factor which takes into account the effect of covalency, ζ ($= 154$ cm^{-1}) is the one-electron spin–orbit parameter, and δ_1, δ_2 and Δ_1 are the separation energies as shown in figure 9. The g-shift of g_z from the free-electron g-value of 2.0023 is smaller than those of g_x and g_y because the energy Δ_1 is much larger than the energies δ_1 and δ_2. The **g**-tensors for the $|yz\rangle$ and $|zx\rangle$ states are calculated in the same way. The g_x-value for the $|yz\rangle$ state and the g_y-value for the $|zx\rangle$ state have the smallest g-shifts.

The observed g-values are $g_x = 1.795(5)$, $g_y = 1.850(5)$ and $g_z = 1.950(5)$ with the principal z axis bent at 30° from the c axis as shown in table 1. Since the g-values are of the order of $2 > g_z > g_y > g_x$, the lowest ground state should be $|xy\rangle$, this result being consistent with the crystal structure of YAP, where the octahedron is compressed along the Al^{3+}–O(III) direction, i.e. the z axis. The parameters λ/δ_1, λ/δ_2 and λ/Δ_1 in equations (3)–(5) are determined to be 0.104, 0.074 and 0.0043, respectively, by fitting the observed g-values to the calculated values. The lowest excited state is $|x^2 - y^2\rangle$. The energy Δ_1 is obtained to be about 20 000 cm^{-1} from the peak energy of band B. Then, the effective spin–orbit parameter λ and the reduction factor k are derived to be 86 cm^{-1} and 0.56, respectively. In the same way, the energy separations of the ground states are $\delta_1 = 830$ cm^{-1} and $\delta_2 = 1160$ cm^{-1}. These values are very similar to those observed for Ti^{3+}:$LaMgAl_{11}O_{19}$ [19].

As the temperature increased, the EPR spectra broadened and finally disappeared above 70 K. This effect is caused by the temperature dependence of the spin–lattice relaxation time T_1 given by [15]

$$1/T_1 = aT + bT^n + c\Delta E^3 \exp(-\Delta E/kT) \quad (6)$$

where ΔE is the energy level of the low-lying excited electronic state. The first term in equation (6) is due to the direct process. The second and third terms are due to the Raman and Orbach processes, respectively, which indicate large temperature dependences. The Orbach process is very important for EPR spectra and includes the term of zero-field splitting of the ground state of paramagnetic ions [13, 15]. As the temperature increases, the second component state of the $^2T_2$ ground state of Ti^{3+}, where ΔE is equal to δ_1 in figure 9, is thermally populated. The lifetime of the lowest orbital component of the $^4T_2$ ground state is associated with the spin–lattice relaxation time T_1. Then, the linewidth of the EPR lineshape is proportional to $1/T_1$. On the assumption that the Raman process in equation (6) is neglected, the linewidth $\Gamma(T)$, normalized by $\Gamma(11)$, is modified by

$$\Gamma(T)/\Gamma(11) = a'T + c' \exp(-\delta_1/kT). \quad (7)$$

The full curve in figure 5(*b*), calculated using equation (7) and the parameters $a' = 0.072$, $c' = 1700$ and $\delta_1 = 170$ cm^{-1}, fits the observed data. A similar

broadening of the EPR spectrum in Ti^{3+}:Al_2O_3 was observed, where the energy separation $\delta_1 \simeq 38$ cm^{-1} [21] and the disappearance temperature $T_{dis} \simeq 12$ K [22]. The factors $\exp(-\delta_1/kT_{dis})$ for Ti^{3+}:YAP and Ti^{3+}:Al_2O_3 are nearly equal, i.e. $\exp[-170/(0.695 \times 55)] \simeq \exp[-38/(0.695 \times 12)]$. The value (170 cm^{-1}) of δ_1 estimated from the spin–lattice relaxation time T_1 is different from that (830 cm^{-1}) obtained from the **g**-tensor. The reason for this large difference may be as follows.

(1) The **g**-tensor of Ti^{3+} is formulated on the assumption of a strong static orthorhombic crystal field, i.e. $\delta_1, \delta_2 \gg \lambda, \hbar\omega$ where $\hbar\omega$ is a phonon energy. When $\delta_1, \delta_2 \simeq \lambda, \hbar\omega$, the g-values may be reduced by the dynamic effect as in the case of Ti^{3+}:Al_2O_3 [21].

(2) We have neglected the Raman process of spin–lattice relaxation.

As described in the above discussion, the energies δ_1 and δ_2 reflect the second and third zero-phonon lines in the emission spectrum, which may be located at positions shifted by amounts of δ_1 and δ_2 towards lower energies from the zero-phonon emission line at 540 nm. The energy δ_1 is denoted by an arrow in the inset in figure 8. The sharp lines at 544.4 nm and 545.4 nm in figure 8 may be due to the second and third zero-phonon levels, respectively, of the $^2T_2$ ground state of Ti^{3+}:YAP. It is, however, reported that the one-phonon spectrum of the luminescence from Cr^{3+}:YAP consists of lines at 78 cm^{-1}, 104 cm^{-1}, 128 cm^{-1}, 136 cm^{-1}, 168 cm^{-1}, 194 cm^{-1}, etc [3]. The luminescence from the accidentally doped Cr^{3+} ions in Ti^{3+}:YAP was observed in the long-wavelength tail of the Ti^{3+} broad-band emission, as shown in figure 8. The spectrum also indicates the phonon structure in the ranges 100–190 cm^{-1} and 250–630 cm^{-1}. Therefore, it seems to be very difficult to distinguish another zero-phonon line and one-phonon line from the structure of the luminescence spectrum of Ti^{3+}:YAP in figure 8.

5. Conclusions

YAP has a slightly distorted perovskite structure with orthorhombic symmetry. The anisotropy of the crystal structure was measured by EPR and polarization of the absorption spectra of Ti^{3+} ions replacing Al^{3+} in YAP. The Ti^{3+} ion is surrounded by six octahedral oxygen ion ligands. The directions towards the oxygen ion ligands are determined from x-ray measurement [8] to be $(\theta_x, \phi_x) = (100°, 56°)$, $(\theta_y, \phi_y) = (80°, 144°)$ and $(\theta_z, \phi_z) = (14°, 17°)$. The principal axes of the Ti^{3+} complex determined by the EPR measurement, $(\theta_x, \phi_x) = (117°, 31°)$, $(\theta_y, \phi_y) = (103°, 127°)$ and $(\theta_z, \phi_z) = (30°, 60°)$, are slightly different from those obtained by x-ray measurement. The energy levels of the ground and excited states of Ti^{3+} have been determined directly from the optical absorption spectrum and the zero-phonon lines in the luminescence spectrum. They have also been derived indirectly from the g-values and the spin–lattice relaxation time of the Ti^{3+} EPR spectra. In consequence, the lowest ground state is determined to be the $|xy\rangle$ state. It has also been deduced from the polarized absorption spectra that the transitions from the lowest ground state, $|xy\rangle$, to the ^2E excited states are caused dominantly by the y component of T_{1u} odd-parity distortion. Although it is difficult to determine precisely the relationship between the T_{1u} distortion and the crystal structure, a comparison of the polarization of the absorption spectra with the theory does indicate which component of the odd-parity distortion is effective in inducing electric dipole transitions between the ground and excited states.

Acknowledgment

The work in Japan was supported in part by a Grant-in-aid (03650032) for Scientific Research from the Ministry of Education, Science and Culture.

References

[1] Kaminskii A A 1990 *Laser Crystals* (Berlin: Springer)
[2] Bass M and Weber M J 1970 *Appl. Phys. Lett.* **17** 395
[3] Weber M J and Varitimos T E 1974 *J. Appl. Phys.* **45** 810
[4] Schepler K L 1986 *Tunable Solid-State Lasers II* ed A B Budgor, L Esterowitz and L G DeShazer (Berlin: Springer) pp 235–9
[5] Wegner T and Petermann K 1989 *Appl. Phys.* B **49** 275
[6] Petermann K 1990 *Opt. Quantum Electron.* **22** S199
[7] Geller S and Wood E A 1956 *Acta Crystallogr.* **9** 563
[8] Diehl R and Brandt G 1975 *Mater. Res. Bull.* **10** 85
[9] Scheare L and Leduc M 1986 *IEEE J. Quantum Electron.* **QE-22** 756
[10] Yamaga M, Henderson B and O'Donnell K P 1990 *J. Lumin.* **46** 397
[11] Yamaga M, Henderson B and O'Donnell K P 1991 *Appl. Phys.* B **52** 122
[12] Yamaga M, Henderson B, O'Donnell K P, Rasheed F, Gao Y and Cockayne B 1991 *Appl. Phys.* B **52** 225
[13] Abragam A and Bleaney B 1970 *Electron Paramagnetic Resonance of Transition Ions* (Oxford: Clarendon) chs 7 and 10
[14] Wertz J E and Bolton J R 1972 *Electron Spin Resonance Elementary Theory and Practical Applications* (New York: McGraw-Hill) ch 12
[15] Pilbrow J R 1990 *Transition Ion Electron Paramagnetic Resonance* (Oxford: Clarendon) chs 3 and 5
[16] Yamaga M, Gao Y, Rasheed F, O'Donnell K P, Henderson B and Cockayne B 1990 *Appl. Phys.* B **51** 329
[17] Sugano S, Tanabe Y and Kamimura H 1970 *Multiplets of Transition Metal Ions in Crystal* (New York: Academic)
[18] Gachter G F and Koningstein J A 1974 *J. Chem. Phys.* **60** 2003
[19] Gourier D, Colle L, Lejus A M, Vivien D and Moncorge R 1988 *J. Appl. Phys.* **63** 1144
[20] Bleaney B and O'Brien M C M 1956 *Proc. Phys. Soc.* B **69** 1216
[21] Macfarlane R M, Wong J Y and Sturge M D 1968 *Phys. Rev.* **166** 250
[22] Kask N E, Kornicko L S, Mandel'shtam T S and Prokhorov A M 1964 *Sov. Phys.–Solid State* **5** 1677